values showed a smaller change in T_2 with temperature change. This finding suggests that lower values of T_2 reflect a smaller scale of molecular motion, with lower activation energies.

Spin–lattice relaxation time (T_1) is known to reflect molecular mobility, similarly to T_2, but increases with decreasing T_2 (with decreasing molecular mobility) in the slow motional regime. The T_1 values of water protons in the presence of drug protons cannot be determined due to spin diffusion, but an approximate determination of T_1 for water protons is possible if the proportion of water protons is large. For example, in $Na_2HPO_4 \cdot 12H_2O$ and $Na_2HPO_4 \cdot 2H_2O$, water protons are predominant (24/25 and 4/5, respectively). $Na_2HPO_4 \cdot 12H_2O$ exhibits slower spin–spin relaxation (larger T_2) (Fig. 12), and faster spin–lattice relaxation (smaller T_1) (Fig. 13) compared to $Na_2HPO_4 \cdot 2H_2O$, which indicates that both T_1 and T_2 reflect the molecular mobility of hydration water. For the antibiotic hydrates examined, however, correlations between T_1 and T_2 were not observed, as shown in Figure 14. This finding indicates that for API hydrates containing a significant amount of drug protons, such as antibiotic hydrates, the molecular mobility of the hydration water is not reflected in T_1.

Hydration Water Showing Gaussian Decay

As mentioned previously, all of the API hydrates other than the four antibiotic hydrates exhibited only Gaussian decay (Fig. 2). The value of T_2 did not vary significantly among the API hydrates, as shown in Figure 15. Furthermore, the onset temperatures of the single endothermic peaks

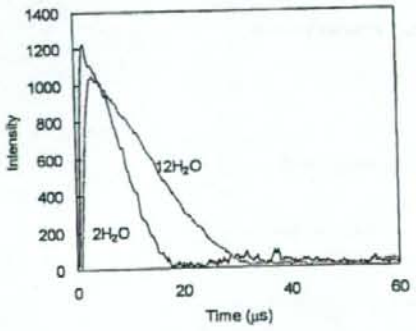

Figure 12. Free induction decay for Na_2HPO_4 $12H_2O$ and $2H_2O$.

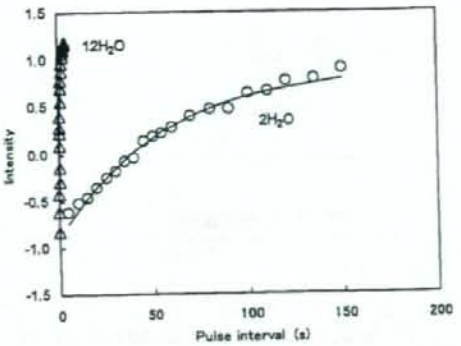

Figure 13. Spin–lattice relaxation for Na_2HPO_4 $12H_2O$ and $2H_2O$.

due to water evaporation for quinidine sulfate, pipemidic acid, and sulpyrine hydrates (Fig. 5), as well as each of the two peaks due to water evaporation observed for quinine hydrochloride, scopolamine hydrobromide, saccharin sodium, and berberine chloride hydrates (Fig. 4), were not correlated with T_2. These findings indicate that the molecular mobility of hydration water that shows Gaussian decay is too low to be reflected in T_2. No correlation between T_2 and molecular mobility is supported by the finding that changes in T_2 associated with changes in temperature were much smaller than those observed for the antibiotic hydrates that exhibited Lorentzian decay, as exemplified by pipemidic acid (Fig. 10). Such low molecular mobility may be attributed to water molecules firmly trapped in the crystal lattice, rather than water molecules trapped in voids in the crystal.

For quinidine sulfate, pipemidic acid, and sulpyrine hydrates, a single endothermic peak was observed in DSC (Fig. 5). The water content versus humidity plots showed a flat line at a certain number of water molecules. Pipemidic acid and sulpyrine showed a flat line at three and one water molecule(s) per hydrate, respectively, and evaporation of these water molecules was observed only under very low humidity (Fig. 7). These findings indicate that water molecules are firmly trapped in the crystal.

For quinine hydrochloride, scopolamine hydrobromide, saccharin sodium, and berberine chloride hydrates, two endothermic peaks were shown in DSC (Fig. 4). The water content versus humidity plots for these hydrates (except for berberine chloride) showed flat lines at two levels

DOI 10.1002/jps

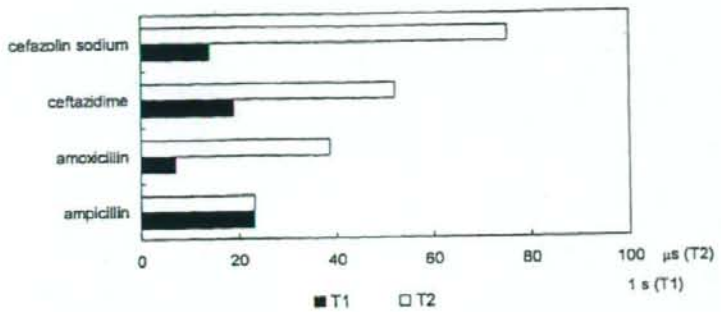

Figure 14. Correlation between T_1 and T_2 for four antibiotic hydrates.

of water content (Fig. 8), suggesting the presence of two water populations: molecules that evaporate at high humidity, and others that evaporate at lower humidity (below 10% RH). This seems to be consistent with the observation of two endothermic peaks in DSC. The endothermic peak observed at a high temperature and the flat line observed at a low humidity may be attributable to hydration water with strong hydrogen–bonding interactions, while the one observed at a lower temperature and higher humidity may be attributable to hydration water with week interactions. The presence of hydration water with week interactions is also supported by the finding that the water contents as measured by the Karl Fischer method were smaller than those specified in the JP (Tab. 1).

CONCLUSION

It was found that spin–spin relaxation time, T_2, is a useful parameter that can indicate the molecular mobility of water of hydration which has relatively high mobility and shows Lorentzian decay upon spin–spin relaxation. For these water molecules, molecular mobility as determined by T_2 is correlated with ease of evaporation both under nonisothermal and isothermal conditions,

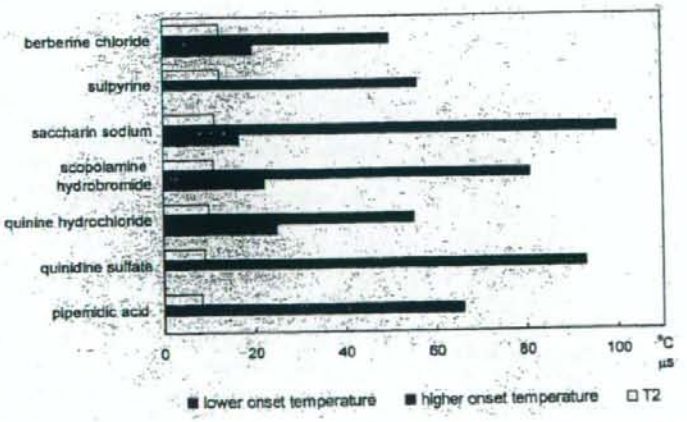

Figure 15. Correlation between onset temperature and T_2 for API hydrates that show Gaussian decay.

such that water molecules with greater ease of evaporation have higher T_2 values.

In contrast, for hydration water that has low mobility and shows Gaussian decay, T_2 was found not to correlate with ease of evaporation under nonisothermal conditions, suggesting that molecular motion that determines the ease of evaporation is not reflected in T_2; in this case, T_2 cannot be used as a parameter to indicate molecular mobility.

The water molecules in the API hydrates studied were found to have wide-ranging molecular mobilities, from low molecular mobility that could not be evaluated by NMR relaxation times, such as the water molecules in pipemidic acid hydrate, to high molecular mobility that could be evaluated by NMR relaxation times, such as the water molecules in ceftazidime hydrate.

REFERENCES

1. Yoshioka S, Aso Y. 2007. Correlations between molecular mobility and chemical stability during storage of amorphous pharmaceuticals. J Pharm Sci 96:960–981.
2. Ahlneck C, Zografi G. 1990. The molecular basis for moisture effects on the physical and chemical stabiity of drugs in the solid state. Int J Pharm 62:87–95.
3. Mimura H, Gato K, Kitamura S, Kitagawa T, Kohda S. 2002. Effect of water content on the solid-state stability in two isomorphic clathrates of cephalosporin: Cefazolin sodium pentahydrte (α form) and KF041 hydrate. Chem Pharm Bull 50: 766–770.
4. Zografi G. 1988. States of water associated with solids. Drug Dev Ind Pharm 14:1905–1926.
5. Newman AW, Reutzel-Edens SM, Zografi G. 2007. Characterization of the "hygroscopic" properties of active pharmaceutical ingredients. J Pharm Sci DOI: 10.1002/jps.21033.
6. Brittain HG, Grant DJW. 1999. Effect of polymorphism and solid state solvation on solubility and dissolution rate. In: Brittain HG, editor. Polymorphism in pharmaceutical solids. New York: Marcel Dekker. pp 279–330.
7. Shinyashiki N, Asaka N, Mashimo S. 1990. Dielectric study on dynamics of water in polymer matrix using a frequency range 10^6–10^{10} Hz. J Chem Phys 93:760–764.
8. Ahlqvist MU, Taylor LS. 2002. Water dynamics in channel hydrates investigated using H/D exchange. Int J Pharm 241:253–261.
9. Ruan R, Chen PL. 1998. Mobility of water in food and biological systems. In: Water in foods and biological materials, a nuclear magnetic resonance approach. Lancaster, PA: Technomic Publishing Company, Inc. pp 149–228.
10. Oksanen CA, Zografi G. 1993. Molecular mobility in mixtures of absorbed water and solid poly(vinylpyrrolidone). Pharm Res 10:791–799.
11. Otsuka T, Yoshioka S, Aso Y, Kojima S. 1995. Water mobility in aqueous solutions of macromolecular pharmaceutical excipients measured by oxygen-17 nuclear magnetic resonance. Chem Pharm Bull 43:1221–1223.
12. Mansfield P. 1965. Multiple-pulse nuclear magnetic resonance transients in solids. Phys Rev 137:A961–A974.
13. Parizel N, Meyer G, Weill G. 1993. Nuclear magnetic resonance linesahape studies of interpenetrating polymer networks. Polymer 12:2495–2502.
14. Morris KR. 1999. Structural aspects of hydrates and solvates. In: Brittain HG, editor. Polymorphism in pharmaceutical solids. New York: Marcel Dekker. pp 125–181.

DOI 10.1002/jps

Glycosylation Analysis of IgLON Family Proteins in Rat Brain by Liquid Chromatography and Multiple-Stage Mass Spectrometry†

Satsuki Itoh,‡ Akiko Hachisuka,‡ Nana Kawasaki,*,‡,§ Noritaka Hashii,‡ Reiko Teshima,‡ Takao Hayakawa,∥ Toru Kawanishi,‡ and Teruhide Yamaguchi‡

Division of Biological Chemistry and Biologicals, National Institute of Health Sciences, 1-18-1, Kamiyoga, Setagaya-ku, Tokyo 158-8501, Japan, Core Research for Evolutional Science and Technology of Japan Science and Technology Agency, Kawaguchi Center Building, 4-1-8 Hon-cho, Kawaguchi, Saitama 332-0012, Japan, and Pharmaceutical Research and Technology Institute, Kinki University, 3-4-1 Kowakae, Higashi-Osaka 577-8502, Japan

Received May 23, 2008; Revised Manuscript Received July 17, 2008

ABSTRACT: IgLON family proteins, including limbic-associated membrane protein (LAMP), opioid-binding cell adhesion molecule (OBCAM), neurotrimin, and Kilon, are immunoglobulin (Ig) superfamily cell adhesion molecules. These molecules are composed of three Ig domains and a glycosylphosphatidylinositol (GPI) anchor and contain six or seven potential N-glycosylation sites. Although their glycosylations are supposed to be associated with the development of the central nervous system like other Ig superfamily proteins, they are still unknown because of difficulty in isolating individual proteins with a high degree of homology in performing carbohydrate analysis. In this study, we conducted simultaneous site-specific glycosylation analysis of rat brain IgLON proteins by liquid chromatography and multiple-stage mass spectrometry (LC−MS^n). The rat brain GPI-linked proteins were enriched and separated by sodium dodecyl sulfate−polyacrylamide gel electrophoresis. The four proteins were extracted from the gel, and subjected to LC−MS^n after proteinase digestions. A set of glycopeptide MS data, including the mass spectrum, the mass spectrum in the selected ion monitoring mode, and the product ion spectra, was selected from all data based on carbohydrate-related ions in the MS/MS spectrum. The peptide portion and the carbohydrate structure were identified on the basis of peptide-related ion and carbohydrate-related ions, and the accurate mass. The site-specific glycosylations of four proteins were elucidated as follows. *N*-Glycans near the N-terminal were disialic acid-conjugated complex- and hybrid-type oligosaccharides. The first Ig domains were occupied by Man-5-9. Diverse oligosaccharides, including Lewis a/x-modified glycans, a brain-specific glycan known as BA-2, and Man-5, were found to be attached to the third Ig domain. Three common structures of glycans were found in the GPI moiety of LAMP, OBCAM, and neurotrimin.

Cell adhesion molecules on cell surfaces are involved in several biological events, such as cell−cell interaction, signaling, and cellular traffic. In the central nervous system, cell adhesion molecules are associated with the differentiation and migration of neurons, and neurite outgrowth. The immunoglobulin (Ig) superfamily, which contains one or more Ig-like domains, is known as one of the cell adhesion molecule families in the central nervous system (*1*). The Ig superfamily includes various proteins, such as P0, Thy-1, myelin-associated glycoprotein (MAG), neural cell adhesion molecule (NCAM), L1, contactin, and IgLON family proteins. Glycosylation of the Ig superfamily proteins is known to be involved in cell−cell interactions (*2*−*4*). Polysialylated glycans in the fifth domain of NCAM are thought to inhibit the interaction of NCAM with other molecules and to promote neural plasticity through a repulsive interaction (*5*, *6*). The HNK-1 epitope in the third and fifth domains of NCAM is known to mediate molecular recognition in the nervous system (*7*).

The IgLON superfamily includes the limbic-associated membrane protein (LAMP),[1] the opioid-binding cell adhesion molecule (OBCAM), neurotrimin, and Kilon (*8*−*14*), and

† This work was supported in part by a Grant-in-Aid from the Ministry of Health and Labor and Welfare, and Core Research for Evolutional Science and Technology Program (CREST) of the Japan Science and Technology Agency (JST).

* To whom correspondence should be addressed: Division of Biological Chemistry and Biologicals, National Institute of Health Sciences, 1-18-1, Kamiyoga, Setagaya-ku, Tokyo 158-8501, Japan. Telephone: +81-3-3700-9074. Fax: +81-3-3707-6950. E-mail: nana@nihs.go.jp.

‡ National Institute of Health Sciences.

§ Core Research for Evolutional Science and Technology of Japan Science and Technology Agency.

∥ Kinki University.

[1] Abbreviations: LC, liquid chromatography; MS, mass spectrometry; MS^n, multiple-stage mass spectrometry; LAMP, limbic-associated membrane protein; OBCAM, opioid-binding cell adhesion molecule; GlcNAc, *N*-acetylglucosamine; GPI, glycosylphosphatidylinositol; PI-PLC, phosphatidylinositol-specific phospholipase C; PNGase F, peptide *N*-glycosidase F; IT-MS, ion trap mass spectrometer; FT ICR-MS, Fourier transform ion cyclotron resonance mass spectrometer; GCC, graphitized carbon column; TIC, total ion chromatogram; CID, collision-induced dissociation; SIM, selected ion monitoring; dHex, deoxyhexose; Hex, hexose; HexNAc, *N*-acetylhexosamine; Fuc, fucose; Man, mannose; Gal, galactose; GlcNAc, *N*-acetylglucosamine; GlcN, glucosamine; NeuAc, *N*-acetylneuraminic acid; $EtNH_2$, ethanolamine; Ino, inositol; BA-2, brain-specific sugar chain, GlcNAcβ1−2Manα1−6(GlcNAcβ1−4)(GlcNAcβ1−2Manα1−3)Manβ1−4GlcNAcβ1−4(Fucα1−6)GlcNAc; SDS−PAGE, sodium dodecyl sulfate−polyacrylamide gel electrophoresis.

10.1021/bi8009778 CCC: $40.75
Published on Web 08/26/2008

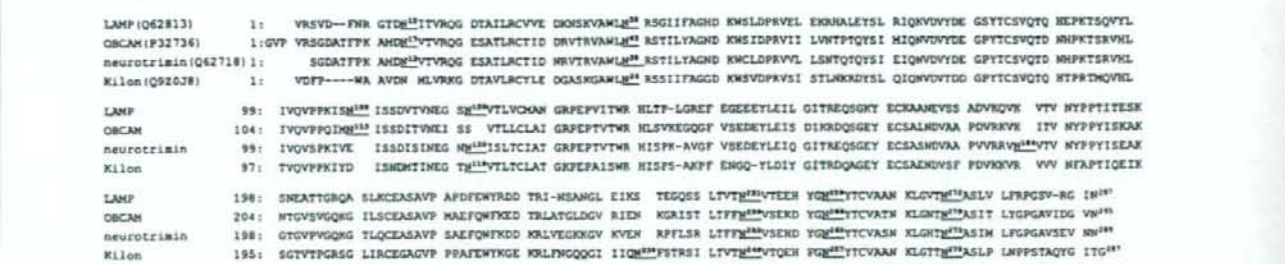

FIGURE 1: Amino acid sequence and potential N-glycosylation sites (in bold) of IgLON family proteins. Their accession numbers in Swiss-prot database are shown in parentheses after their names. The C-terminal amino acids in the proteins are predicted GPI attachment sites.

these proteins are distributed differently in the central nervous system during the development of neurons in a brain (*11*, *13*−*18*). The IgLON family proteins consist of three Ig domains, the third of which is attached to a glycosylphosphatidylinositol (GPI) anchor. Each of the IgLON family proteins includes six or seven consensus N-glycosylation sites (Figure 1), and the glycosylation is presumed to play essential roles in the neural circuit formation like other Ig superfamily proteins (*2*−*4*). However, since the high degree of homology of their amino acid sequences makes it difficult to isolate the individual proteins of this family to perform carbohydrate analysis, their glycosylation features are still unknown with the exception of a linkage of *N*-glycans in OBCAM and Kilon and of high mannose-type and hybrid-type oligosaccharides in LAMP (*9*, *18*, *19*).

Recently, liquid chromatography and mass spectrometry (LC−MS) and liquid chromatography and multiple-stage mass spectrometry (LC−MS^n) have been widely applied to the site-specific glycosylation analysis of a glycoprotein (*20*−*24*). Generally, a tryptic digest of an isolated glycoprotein is separated with a reversed-phase or normal-phase column, and the separated glycopeptides are directly subjected to MS and MS^n (*25*−*27*). The site-specific glycosylation is deduced from the mass spectra of the glycopeptides, and the sequences of both the peptide and carbohydrate portions are deduced from the fragment ions in the MS^n spectra. Using this technique, we previously performed a site-specific glycosylation analysis of rat brain Thy-1, which contains three N-glycosylation sites and a GPI anchor (*28*). GPI-anchored proteins enriched via phase partitioning with Triton X-114 and PIPLC digestion were separated by SDS−PAGE, and the Thy-1 protein extracted from the gel was digested with trypsin or endoproteinase Asp-N. The Thy-1 glycopeptides were separated and analyzed by using a liquid chromatography and ion trap mass spectrometer (IT-MS) equipped with a C18 column. The peptide portions of glycopeptides were identified on the basis of the *m*/*z* values of the peptide-related ions and the b- and y-ions that arose from the peptide backbone. The carbohydrate structures at each glycosylation site and in the GPI moiety were successfully determined from fragment ions in the MS/MS spectra. This result suggests that LC−MS^n can be effectively utilized for site-specific glycosylation analysis of each glycoprotein in the mixture of several glycoproteins simultaneously.

In this study, we conducted site-specific glycosylation analyses of rat LAMP, OBCAM, neurotrimin, and Kilon using LC−MS^n. The GPI-linked proteins in the rat brains were separated by SDS−PAGE, and the IgLON family proteins were extracted from a gel band (45−70 kDa). The mixture of proteins was digested with proteinases, and the site-specific glycosylation analysis of the four proteins was performed by using an ion trap-Fourier transform ion cyclotron resonance mass spectrometer (IT-MS-FT ICR-MS), which is capable of acquiring the accurate mass as well as the MS^n spectra. We successfully elucidated the site-specific glycosylation and the structure of the GPI moieties of LAMP, OBCAM, neurotrimin, and Kilon. This is the first report of the simultaneous site-specific glycosylation analysis of four similar glycoproteins.

EXPERIMENTAL PROCEDURES

Materials. The rat brains (Wister, male, 3 weeks old) were purchased from Nippon SLC (Hamamatsu, Japan). Phosphatidylinositol-specific phospholipase C (PIPLC) from *Bacillus cereus* was obtained from Molecular Probes (Eugene, OR). Trypsin-Gold was purchased from Promega (Madison, WI). PNGase F and endoproteinase Glu-C were purchased from Roche Diagnostics (Mannheim, Germany). SimplyBlue SafeStain was obtained from Invitrogen (Carlsbad, CA). All other chemicals were of the highest available purity.

SDS−PAGE of Enriched Lipid-Free GPI-Linked Proteins. Lipid-free GPI-linked proteins were enriched from rat brain as reported previously (*28*, *29*). Briefly, the homogenate of two rat brains (total wet weight of 1.4 g) was defatted and solubilized with 2% Triton X-114 at 4 °C overnight (*29*, *30*). After centrifugation, the supernatant was subjected to Triton X-114 phase partitioning at 37 °C. Cold acetone was added to the detergent phase containing solubilized membrane proteins, and the resulting precipitate was digested with PIPLC. After the PIPLC digest mixture had been subjected to Triton X-114 phase partitioning, lipid-free GPI-linked proteins in the aqueous phase were precipitated via addition of cold acetone. These proteins were separated by SDS−PAGE (12.5%) (brain wet weight of 50 mg/lane) after carboxyamidomethylation (*31*) and detected after being stained with Coomassie Brilliant Blue G-250 using SimplyBlue SafeStain.

Protein Identification. Gel-separated proteins were extracted after in-gel trypsin digestion as previously reported (*32*) and subjected to LC−MS/MS with a Paradigm MS4 HPLC system (Michrom BioResources, Inc., Auburn, CA) consisting of pump A with 0.1% formic acid and 2% acetonitrile and pump B with 0.1% formic acid and 90% acetonitrile. Peptides were separated with a Magic C18 column (50 mm × 0.2 mm, 3 μm; Michrom BioResources Inc.) with a linear gradient from 5 to 65% of pump B over

20 min at a flow rate of 3 μL/min. Mass spectra were recorded with a Finnigan LTQ system (Thermo Fisher Scientific, Waltham, MA) using sequential scan events: MS (*m/z* 450−2000) followed by data-dependent MS/MS on the IT-MS for the most intense ions in positive ion mode. For protein identification, all obtained product ions were subjected to a computer database search analysis with the TurboSEQUEST search engine (Thermo Fisher Scientific) using the Swiss-Prot database and search parameters: a static modification of carboxyamidomethylation (57 Da) at Cys and trypsin for digestion.

Extraction and Proteinase Digestion of the 45−70 kDa Proteins Separated by SDS−PAGE. The gel-separated proteins were extracted as previously reported (*28*). The proteins were extracted with 20 mM Tris-HCl containing 1% SDS by being shaken vigorously overnight after the gel had been broken down into small bits. The extract was filtered with Ultrafree-MC (0.22 μm; Millipore, Bedford, MA), and the proteins were precipitated via addition of cold acetone. The resulting precipitate was digested with endoproteinase Glu-C (3.75 μg) in 30 μL of 0.1 M ammonium acetate (pH 8.0) at 37 °C for 4 days, followed by incubation with additional trypsin (1 μg) at 37 °C overnight.

LC−MS^n. Proteolytic peptides were separated by reversed-phase columns, Magic C30 and C18 (50 mm × 0.1 mm, 3 μm; Michrom BioResources), and a graphitized carbon column (GCC), Hypercarb 5 μ (150 mm × 0.2 mm; Thermo Fisher Scientific), with a Paradigm MS4 HPLC system consisting of pump A with 0.1% formic acid and 2% acetonitrile and pump B with 0.1% formic acid and 90% acetonitrile. For analysis of glycopeptides, separation was performed with a linear gradient from 5 to 50% pump B over 100 min followed by a 50 to 95% B gradient over 10 min and 95% B over 10 min at a flow rate of 0.5 μL/min, and mass spectra were recorded with a Finnigan LTQ-FT system (Thermo Fisher Scientific) using sequential scan events: MS (*m/z* 1000−2000 or 700−2000) with the IT-MS followed by MS with the IT-MS-FT ICR-MS in selected ion monitoring (SIM) mode and data-dependent MS^n with the IT-MS for the most intense ions. The LC−MS^n runs were performed with a C30 column and scan range of *m/z* 1000−2000 (condition A), twice, with a C30 column and scan range of *m/z* 700−2000 (condition B), once, and with a C18 column and scan range of *m/z* 1000−2000 (condition C), once. For analysis of GPI-linked peptides, separation was performed with a linear gradient from 5 to 60% pump B over 100 min at a flow rate of 2 μL/min for a GCC, and mass spectra were recorded with a Finnigan LTQ system using sequential scans: a single mass scan (*m/z* 700−2000) with the IT-MS followed by data-dependent MS^n scans with the IT-MS for the most intense ions, twice. LC−MS^n was performed using a capillary voltage of 1.8 kV and a capillary temperature of 200 °C.

RESULTS

Preparation of Lipid-Free IgLON Glycopeptides. Figure 2 illustrates the experimental procedure for the glycosylation analysis of IgLON family proteins. Lipid-free GPI-linked proteins in a rat brain tissue sample were enriched via phase partitioning with Triton X-114 and PIPLC digestion. The enriched proteins were separated by SDS−PAGE and stained

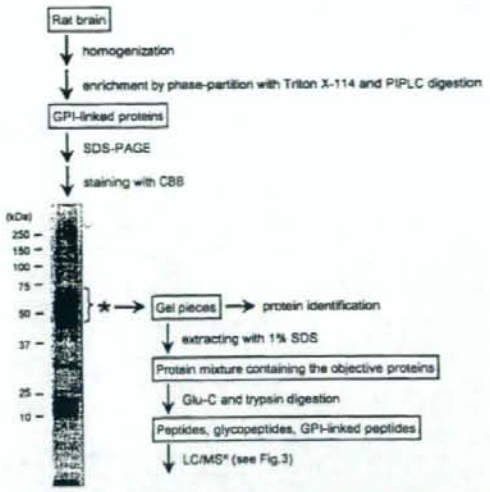

FIGURE 2: Experimental procedure for site-specific glycosylation analysis of IgLON family proteins and SDS−PAGE (12.5%) of lipid-free GPI-linked proteins which were enriched from rat brain. The asterisk indicates the gel band containing IgLON family proteins.

with Coomassie Brilliant Blue. The presence of LAMP, OBCAM, neurotrimin, and Kilon in the gel band at 45−70 kDa was confirmed by in-gel trypsin digestion followed by LC−MS/MS. The IgLON proteins were extracted with other comigrated proteins from 45−70 kDa bands in other lanes by being shaken in 1% SDS. After SDS had been removed, the mixture of proteins was digested with endoproteinase Glu-C and trypsin. Most of the resulting glycopeptides contained only a single N-glycosylation site, with the exception of LGTTN^{270}ASLPLNPPSTAQYGITG^{287} in Kilon, which included a predicted GPI attachment site at Gly287 in addition to a potential N-glycosylation site at Asn270 (Figure 1). The glycopeptides from IgLON family proteins was separated by using three different columns: a reversed-phase column, a C30 and a C18 column for hydrophobic glycopeptides, and a GCC for hydrophilic glycopeptides, including GPI-linked peptides.

Glycosylation Analysis of LAMP. LC−MS analysis was performed via MS on the IT-MS and data-dependent MS in SIM mode on the FT ICR-MS, and data-dependent MS/MS and MS/MS/MS were performed on the IT-MS in the positive ion mode (Figure 3). After MS data acquisition, the MS/MS spectrum (scan *n*) of a glycopeptide was selected manually from all MS data on the basis of the existence of carbohydrate distinctive fragments, such as $Hex_1HexNAc_1^+$ (*m/z* 366) and $Hex_1HexNAc_1NeuAc^+$ (*m/z* 657). Then a set of the glycopeptide's MS data consisting of the mass spectrum (scan $n-2$), the mass spectrum in SIM on the FT ICR-MS (scan $n-1$), the MS/MS spectrum (scan *n*), and the MS/MS/MS spectrum (scan $n+1$) was selected from all the MS data (step 1). The carbohydrate structure was deduced from the fragment ions appearing in the MS/MS spectrum (scan *n*), and the peptide portion was estimated from the peptide-related ions (step 2). The sequences of some peptides were confirmed by the b- and y-ions that arose from Y_1 ([peptide + HexNAc + H]$^+$) in MS/MS/MS (scan $n+$

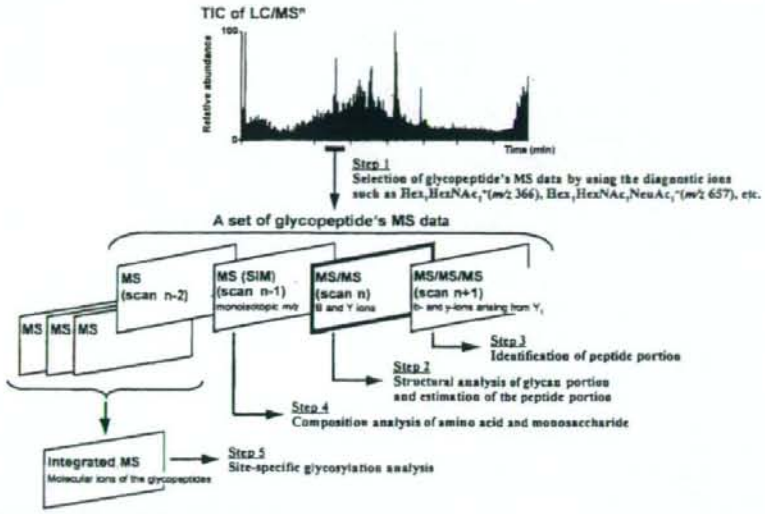

FIGURE 3: Methods used for LC−MS^n and data analysis.

1) (step 3). The accurate molecular mass that was calculated from the monoisotopic m/z value and the charge state acquired by FT ICR-MS in SIM mode (scan n − 1) was used to corroborate the assignment of the peptide and glycan moieties (step 4). The mass spectra acquired at the elution position, where the glycopeptides that yielded identical Y_1 ions in the MS/MS and/or MS/MS/MS spectra, were integrated, and the site-specific glycosylation was elucidated on the basis of the distribution of molecular ions in the integrated mass spectra (step 5). As a representative separation pattern, a total ion chromatogram (TIC) obtained by LC−MS^n with a C30 column (scan range of m/z 1000−2000) is shown in Figure 4A. The MS/MS spectra containing the diagnostic ions at m/z 366 and 657 were picked out from all the MS data, and the peptides eluted at positions 1−25 were determined to be the glycopeptides on the basis of the carbohydrate-related ions. The 19% of spectra acquired at elution time, including positions 1−25, could be traced back to the glycopeptides of IgLON family proteins.

As for LAMP, it has seven potential N-glycosylation sites at Asn12, -38, -108, -120, -251, -259, and -272, and Asn287 is the predicted site of GPI linkage. On the basis of the presence of the peptide-related ions ([peptide + HexNAc + H]$^+$, Y_1 or $Y_{1\alpha/\beta}$; or [peptide + dHex-HexNAc + H]$^+$, $Y_{1\alpha}$), glycopeptides that were eluted at the positions 1, 11, 14, 12, 4, and 24 were estimated to be the glycopeptides containing Asn12, -38, -108, -251, -259, and -272, respectively. The MS/MS spectra of the glycopeptide containing Asn120 (GSN^{120}VTLVCMANGRPE) were not acquired in any of the runs. However, glycosylation at Asn120 was confirmed by the detection of the peptide substituted with Asp (GSD^{120}VTLVCMANGRPEPVITWR) after PNGase F digestion (data not shown). Panels A1−F1 of Figure 5 show the representative MS/MS and MS/MS/MS spectra acquired at positions 11, 1, 14, 12, 4, and 24, respectively. The integrated mass spectra of the glycopeptides containing Asn38, -12, -108, -251, -259, and -272 are shown in panels A2−F2 of Figure 5, respectively. The feature of the glycosylation at each glycosylation site was elucidated on the basis of these MS spectra.

(i) Asn38 (Asn43 in OBCAM and Asn38 in neurotrimin). Panel A1 of Figure 5 shows one of the MS/MS spectra acquired at position 11. The peptide portion, VAWL(GlcNAc-)N^{38}R, was confirmed on the basis of the b- and y-ions that arose from Y_1 (m/z 961.5) in the MS/MS/MS spectrum (panel A1″ of Figure 5). A series of doubly charged Y ions with an m/z spacing pattern, 81 m/z units (Hex), suggests the linkage of Man-7 to this peptide. The attachment of Man-7 to VAWLN^{38}R, whose theoretical monoisotopic m/z value ([M + 2H]$^{2+}$) is 1149.983, was ascertained by the observed monoisotopic m/z value (1149.986) acquired in SIM mode on the FT ICR-MS (panel A1′ of Figure 5). Panel A2 of Figure 5 shows the integrated mass spectrum which was obtained from the mass spectra of glycopeptides that yielded Y_1 (m/z 961.5) via MS/MS. Four noticeable ion peaks (peaks a-1−a-4) appearing with the differences of 81 m/z units are assigned to VAWLN^{38}R glycosylated with Man-6-9 (Table 1A). The MS/MS spectra of DKNSKVAWLN^{38}R and CVVEDKNSKVAWLN^{38}R, which were picked out from positions 9 and 15, also revealed that Man-5, -7, and -8 were attached to Asn38.

(ii) Asn12. Panel B1 of Figure 5 shows the representative MS/MS spectrum of glycopeptide, GTDN^{12}ITVR, which was selected from position 1. From the $Y_{1\alpha}$ ion (m/z 1224.5) together with monoisotopic m/z value of the molecular ion (m/z 1173.132) and a series of doubly charged Y ions with an m/z spacing pattern, 146 (NeuAc), 101 (HexNAc), and 81 m/z units (Hex), the carbohydrate portion was estimated to be dHex$_1$Hex$_5$HexNAc$_4$NeuAc$_4$. Furthermore, a complex-type oligosaccharide, to which one branch of disialic acid was attached, was deduced from the presence of $B_{4\alpha}/Y_{5\alpha'}$ (m/z 495.3), $B_{2\alpha}$ (m/z 582.7), $B_{3\alpha}$ (m/z 744.9), $B_{4\alpha}/Y_{5\alpha''}$ and $B_{4\alpha}/Y_{7\alpha'}$ (m/z 948.2), and $B_{4\alpha}$ (m/z 1239.5) (inset of panel B1 of Figure 5). The integrated mass spectrum at position 1 suggests that the majority of the glycans at Asn12 are hybrid- and complex-type oligosaccharides containing disialic acids

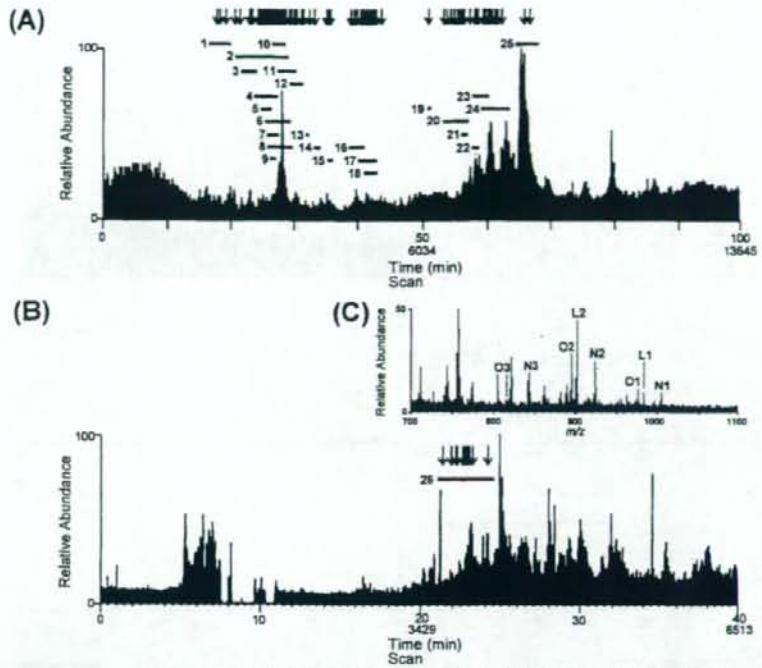

FIGURE 4: Total ion chromatograms obtained by C30-LC−MS^n (A) and GCC-LC−MS^n (B). Lines 1−25 and 26 are the elution positions of glycopeptides and GPI-linked peptides, respectively. The down arrow denotes the extracted position of the MS/MS spectra. (C) Integrated mass spectrum obtained from elution position 26. L1 and L2 are molecular ions of GPI-linked peptides from LAMP, N1−N3 those from neurotrimin, and O1−O3 those from OBCAM.

(panel B2 of Figure 5 and Table 1B). In addition, the partial glycosylation at Asn12 was indicated by the detection of nonglycosylated GTDN^{12}ITVR.

(iii) Asn108. The MS/MS spectrum of glycosylated ISN^{108}ISSDVTVNE ($Y_{1\alpha/1\beta}$, *m/z* 1480.6) acquired at position 14 is shown in panel C1 of Figure 5. The attachment of a Lewis a/x [Le$^{a/x}$, Gal-(Fuc-)GlcNAc-] or H antigen (Fuc-Gal-GlcNAc-) motif to the bisected complex-type oligosaccharide was deduced from the monosaccharide composition ($dHex_2Hex_4HexNAc_5$) and the Le$^{a/x}$ and H antigen-related ion (*m/z* 512.1) and $Y_{1\beta/3\alpha/3\beta}{}^{2+}$ (*m/z* 1024.3) (panel C1 of Figure 5, peak c-1 in panel C2 of Figure 5). The alternative LC−MS^n run with the C30 column (scan range of *m/z* 1000−2000) suggested that ISN^{108}ISSD is also occupied by sialyl Le$^{a/x}$ (sLe$^{a/x}$)-modified or core-fucosylated hybrid-type oligosaccharides based on the presence of NeuAc-Hex-(dHex-)HexNAc$^+$ (*m/z* 803.1), Hex-(dHex-)HexNAc$^+$ (*m/z* 512.3), NeuAc-Hex$^+$ (*m/z* 454.2), and [peptide + dHex + HexNAc + H]$^+$ (*m/z* 1084.3) (data not shown, Table 1C).

(iv) Asn251. The representative MS/MS spectrum of the glycopeptide containing GQSSLTVTN^{251}VTE ($Y_{1\alpha/1\beta}$, *m/z* 1438.6; elution position 12) is shown in panel D1 of Figure 5. From the monoisotopic mass and the Le$^{a/x}$-related ions (*m/z* 350.3 and 512.2), the carbohydrate structure was estimated to be a complex-type oligosaccharide to which the Le$^{a/x}$ motif was attached ($dHex_2Hex_4HexNAc_5$; inset of panel D1 of Figure 5). Other glycans at Asn251 were characterized as complex-type oligosaccharides containing sLe$^{a/x}$ or Lewis b/y [Le$^{b/y}$, Fuc-Gal-(Fuc-)GlcNAc-] based on the molecular ions in the integrated mass spectrum (peaks d-1−6 in panel D2 of Figure 5), the sLe$^{a/x}$-related ions (*m/z* 803, 657, and 512), and the Le$^{b/y}$-related ions (*m/z* 658.2, 512.1, and 350.2) acquired by the alternative run with the C30 column (scan range of *m/z* 700−2000) (Table 1D).

(v) Asn259. Panel E1 of Figure 5 shows the product ion spectra of HYGN^{259}YTCVAANK linked by $dHex_1Hex_3HexNAc_5$, which was deduced from the $Y_{1\alpha/1\beta}$ ion (*m/z* 1600.6) and the monoisotopic mass acquired at position 4. The BA-2, which is a core-fucosylated and agalacto-biantennary oligosaccharide with bisecting GlcNAc, and known as a brain-specific carbohydrate, was suggested by the product ions at *m/z* 1085.3 (bisecting GlcNAc) and 1746.6 (core-fucosylation) (inset of panel E1 of Figure 5). The majority of other glycans at Asn259 were characterized as Le$^{a/x}$-modified complex and hybrid types. Man-5 was suggested to be a minor glycan (panel E2 of Figure 5 and Table 1E).

(vi) Asn272. Panel F1 of Figure 5 shows the MS/MS and MS/MS/MS spectra of glycopeptide LGVTN^{272}ASLVLFR ($Y_{1\alpha/1\beta}$, *m/z* 1492.8), which were acquired at position 24. The monosaccharide composition ($dHex_2Hex_4HexNAc_5$) and the presence of $Y_{3\alpha/3\beta}{}^{2+}$ (*m/z* 1103.8) and Le$^{a/x}$-related ion suggested the attachment of a Le$^{a/x}$ or H antigen motif to the bisected and core-fucosylated complex-type oligosaccharide (inset of panel F1 of Figure 5). The MS/MS spectra of the LGVTN^{272}ASLVLFRPGSVR glycopeptides ($Y_{1\alpha/1\beta}{}^{2+}$, *m/z* 1069) were also picked out at position 24 (data not shown). The *m/z* values of molecular ions appearing in the

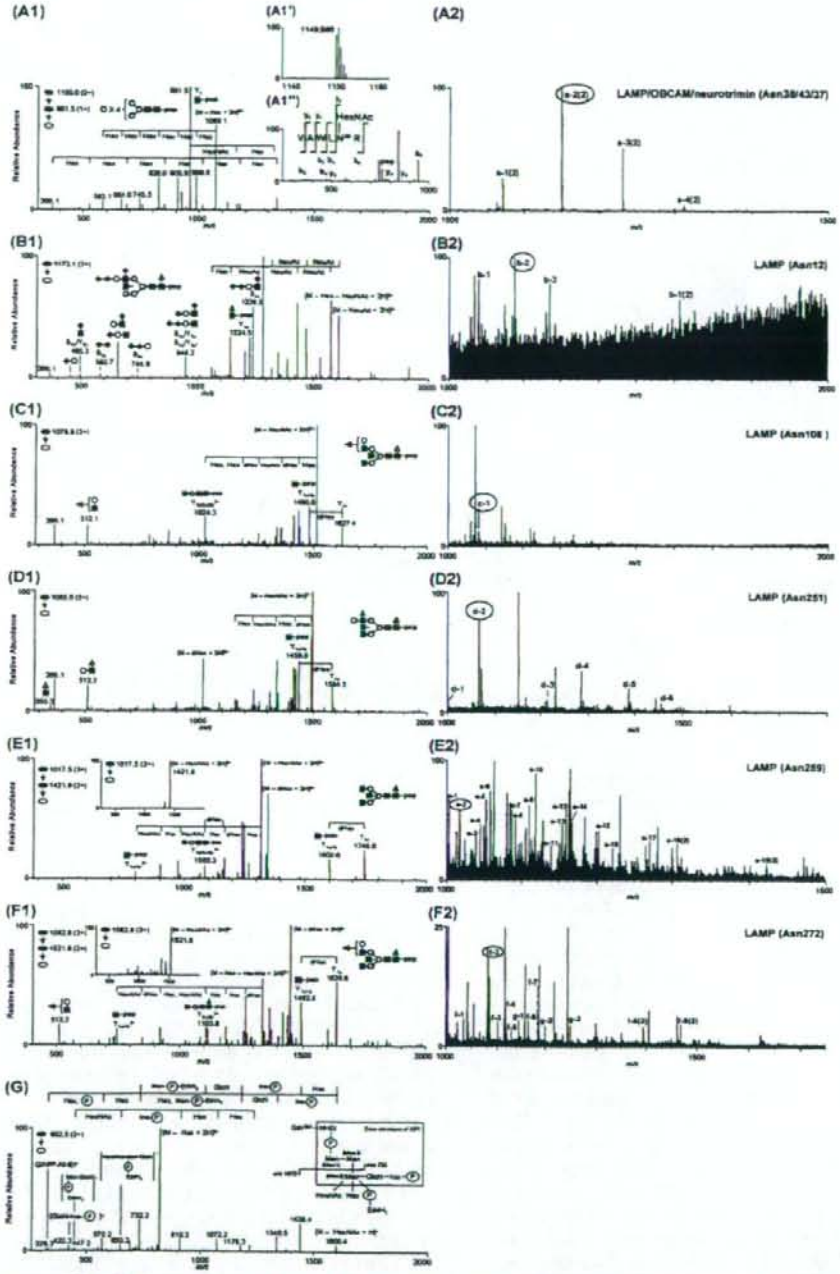

FIGURE 5: MS spectra of LAMP glycopeptides. (A1) MS/MS spectrum of glycopeptide VAWLN[38]R; elution position, 11; precursor ion, $[M + 2H]^{2+}$ (m/z 1150.0). (A1') Mass spectrum on the FT ICR-MS in SIM mode. (A1'') MS/MS/MS spectrum acquired from Y_1 (m/z 961.5). (A2) Integrated mass spectrum obtained from position 11. (B1) MS/MS spectrum of glycopeptide GTDN[12]ITVR; elution position, 1; precursor ion, $[M + 3H]^{3+}$ (m/z 1173.1). (B2) Integrated mass spectrum at position 1. (C1) MS/MS spectrum of glycopeptide ISN[108]ISSDVTVNE; elution position, 14; precursor ion, $[M + 3H]^{3+}$ (m/z 1078.8). (C2) Integrated mass spectrum at position 14. (D1) MS/MS spectrum of glycopeptide GQSSLTVTN[251]VTE; elution position, 12; precursor ion, $[M + 3H]^{3+}$ (m/z 1065.0). (D2) Integrated mass spectrum at position 12. (E1) MS/MS and MS/MS/MS spectra of glycopeptide HYGN[259]YTCVAANK; elution position, 4; precursor ion, $[M + 3H]^{3+}$ (m/z 1017.5). (E2) Integrated mass spectrum at position 4. (F1) MS/MS and MS/MS/MS spectra of glycopeptide LGVTN[272]ASLVLFR; elution position, 24; precursor ion, $[M + 3H]^{3+}$ (m/z 1082.8). (F2) Integrated mass spectrum at position 24. (G) MS/MS spectrum of GPI-linked GIN[287]; elution position, 26; precursor ion, $[M + 2H]^{2+}$ (m/z 902.5). Symbols are as in Figure 9.

Table 1: Summary of Glycosylation Analysis of IgLON Family Proteins

protein	peptides:	sequence[a,b]	elution position	Figure	glycopeptides: peak no.[c]	scan in Figure 4A[d]	observed peptide-related ion[e]	observed m/z in SIM mode[b]	theoretical m/z[b]	N-glycan: deduced monosaccharide composition: dHex	Hex	HexNAc	NA	deduced structure[f] (diagnostic ion)
LAMP	B	GTDN[51]ITVR (874.451)	1	5, B2	b-1	2095 (A, B)	1225.4	1076.101 (3)	1076.101	1	5	4	2	H, CoreF(1225.4)
					b-1 (2)	2146	1225.6	1613.652 (2)	1613.648	1	5	4	2	H, CoreF(1225.6)
					b-2	**2166 (A, B, C)**	**1224.5**	**1173.132 (3)**	**1173.133**	**1**	**5**	**4**	**3**	**H, CoreF(1224.5), diSia(582.7) [Figure 5, B1]**
						– (A)	1224.5	1759.195 (2)	1759.196	1	5	4	3	CoreF(1224.5), diSia(583.0)
					b-3	2235 (A)	1224.5	1270.166 (3)	1270.165	1	5	4	4	C, CoreF(1224.5), diSia(583.0)
						– (A)	1225.6	1367.199 (3)	1367.196	1	5	4	5	C, CoreF(1225.6), diSia(583.4)
	A	VAWLN[38]R (757.424)	11	5, A2		– (B)	961.5	987.930 (2)	987.930	0	5	2	0	Man-5
					a-1 (2)	3523 (A, B, C)	961.5	1068.956 (2)	1068.957	0	6	2	0	Man-6
					a-2 (2)	**3364 (A, B, C)**	**961.5**	**1149.986(2)**	**1149.983**	**0**	**7**	**2**	**0**	**Man-7 [Figure 5, A1]**
					a-3 (2)	3221 (A, B, C)	961.5	1231.010 (2)	1231.010	0	8	2	0	Man-8
					a-4 (2)	3413 (A, B, C)	961.5	1312.039 (2)	1312.036	0	9	2	0	Man-9
		DKNSKVAWLN[38]R (1329.715)	9	–	–	3074	1534.8	1011.774 (3)	1011.773	0	8	2	0	Man-8
		CVVEDKNSKVAWLN[38]R (1816.925)	15	–	–	4298	675.5(3)	1012.128 (3)	1012.123	0	5	2	0	Man-5
					–	4245	1011.2(2)	1120.160 (3)	1120.159	0	7	2	0	Man-7
					–	4208	1011.3(2)	1174.175 (3)	1174.176	0	8	2	0	Man-8
	C	ISN[166]ISSD (734.345)	–	–		– (A)	938.4	1296.508 (2)	1296.507	1	5	3	1	H, CoreF(1084.3) or sL[a/b] (454.2, 512.3, 657.2, 803.1)
						– (A)	938.5	1377.533 (2)	1377.534	1	6	3	1	H, CoreF(1084.2)
		ISN[166]ISSDVTVNE (1276.615)	14	5, C2	c-1	**3963**	**1480.6**	**1078.456 (3)**	**1078.454**	**2**	**4**	**5**	**0**	**C, CoreF(1627.4), bisectGN(1024.3) [Figure 5, C1]**
		GSN[120]VTLVCMANGRPEPVITWR (1603.745)	–	–	–	–	–	–	–	–	–	–	–	glycosylated [g]
	D	GQSSLTVTN[251]VTE (1234.604)	12	5, D2		– (A)	1438.6	1340.576 (2)	1340.576	1	3	4	0	CoreF(1584.6), bisectGN(1003.6)
						– (A)	1438.5	961.746 (3)	961.746	1	3	5	0	C, CoreF(1584.5), bisectGN(1004.1), BA-2
						– (A, B)	1438.5	1442.115 (2)	1442.116	1	3	5	0	C, CoreF(1584.5), bisectGN(1077.2), BA-2
					d-1	3630	1438.5	1002.088 (3)	1002.088	1	5	4	0	H, CoreF(1584.5) or L[x/y] (350.1, 512.1)
					d-2	**3646 (A, B, C)**	**1438.6**	**1064.451 (3)**	**1064.450**	**2**	**4**	**5**	**0**	**C, CoreF(1584.5), L[x/y] (350.3, 512.2) [Figure 5, D1]**
						– (C)	1439.6	1596.174 (2)	1596.171	2	4	5	0	C, CoreF(1585.6), 512(512.2)
						– (B)	1438.5	1167.154 (3)	1167.154	3	5	5	0	C, CoreF(1584.5), bisectGN(1004.1), L[x/y] (350.2, 512.1, 658.2)
					d-3	3742 (C)	1438.6	1215.502 (3)	1215.499	2	5	5	1	C, CoreF(1584.4), 512(512.3)
					d-4	3788 (C)	1438.6	1283.192 (3)	1283.193	2	5	6	1	C, CoreF(1584.5) (sL[x/y] (512.2, 657.2, 803.2))
					d-5	3668	1438.6	1385.898 (3)	1385.896	3	6	6	1	C, CoreF(1584.5) (sL[x/y] (512.2, 657.3, 803.1))
					d-6	3618 (A)	1438.5	1453.594 (3)	1453.589	3	6	7	1	C, CoreF(1584.6), 512(512.2)

Table 1: Continued

peptides		glycopeptides							*N*-glycan				
									deduced monosaccharide composition				
protein	sequence[a,b]	elution position	Figure	peak no.[c]	scan in Figure 4A[d]	observed peptide-related ion[e]	observed *m/z* in SIM mode[b]	theoretical *m/z*[b]	dHex	Hex	HexNAc	NA	deduced structure[f] (diagnostic ion)
E	HYGN[155]YTCVAANK (1396.619)	4	5, E2		– (B)	801.8(2)	872.021 (3)	872.021	0	5	2	0	Man-5
				e-18 (2)	2884	1600.6	1307.532 (2)	1307.528	0	5	2	0	Man-5
				e-19 (2)	2949 (A)	1601.4	1421.587 (2)	1421.584	1	3	4	0	CoreF(1746.7), bisectGN(1085.6)
				e-1	2891 (A, C)	1600.6	1002.079 (3)	1002.076	1	4	4	0	H, CoreF(1746.6), bisectGN(1085.3)
				e-2	**2931 (A, B, C)**	**1600.6**	**1015.752 (3)**	**1015.752**	**1**	**3**	**5**	**0**	**C, CoreF(1746.6), bisectGN(1085.3), BA-2 [Figure 5, E1]**
				e-3	2859 (A)	1600.5	1037.089 (3)	1037.086	2	5	3	0	H, CoreF(1746.6), 512(512.1)
				e-4	2840	1600.6	1042.419 (3)	1042.418	1	6	3	0	H, 512(512.1)
				e-5	2878 (A)	1601.6	1050.764 (3)	1050.762	2	4	4	0	CoreF(1746.6), $L^{a/x}$ (350.2, 512.2), bisectGN(1085.5)
				e-6	2853 (A, B, C)	1600.5	1056.095 (3)	1056.094	1	5	4	0	H, CoreF(1747.7), bisectGN(1085.6)
				e-7	2994	1600.7	1085.433 (3)	1085.432	1	5	3	1	H, CoreF(1747.6) or 512(512.2)
				e-8	2821	1600.5	1091.107 (3)	1091.104	2	6	3	0	H, CoreF(1746.6), 512(512.2)
					– (A, C)	1601.6	1104.779 (3)	1104.780	2	5	4	0	H, CoreF(1747.8), bisectGN(1158.7), $L^{a/x}$ (349.9, 512.3)
				e-9	2847	1600.6	1110.111 (3)	1110.111	1	6	4	0	H, CoreF(1746.6) or $L^{a/x}$ (350.1, 512.3)
				e-10	2898 (A, C)	1601.7	1118.457 (3)	1118.455	2	4	5	0	C, CoreF(1746.7), bisectGN(1085.7), $L^{a/x}$ (350.2, 512.1)
				e-11	2989	1600.7	1139.452 (3)	1139.450	1	6	3	1	H, CoreF(1746.7)
				e-12	2808 (A)	1600.6	1153.467 (3)	1153.466	3	5	4	0	C, CoreF(1746.6), $L^{b/y}$ (658.2) or 512/512(512.1/512.3)
				e-13	2872	1600.4	1158.798 (3)	1158.797	2	6	4	0	H, CoreF(1747.7), $L^{a/x}$ (350.1, 512.1)
				e-14	3036	1601.7	1166.800 (3)	1166.801	1	4	5	1	C, CoreF(1747.4) or 512(512.1), bisectGN(1085.3)
				e-15	2983	1600.6	1201.813 (3)	1201.811	2	5	4	1	C, CoreF(1747.6), $sL^{a/x}$ (350.1, 512.2, 657.3, 803.2)
				e-16	2815	1600.6	1221.160 (3)	1221.159	3	5	5	0	C, CoreF(1747.6), bisectGN(1085.3), 512(512.2)
				e-17	3013	1600.7	1269.507 (3)	1269.505	2	5	5	1	C, CoreF(1746.7), bisectGN(1085.5), 512(512.1)

Table 1: Continued

protein	peptides: sequence[a,b]	elution position	Figure	glycopeptides: peak no.[c]	scan in Figure 4A[d]	observed peptide-related ion[e]	observed m/z in SIM mode[b]	theoretical m/z[b]	N-glycan: deduced monosaccharide composition dHex	Hex	HexNAc	NA	deduced structure[f] (diagnostic ion)
F	LGVTN[372]ASLVLFR (1288.750)	24	5, F2		– (B)	1492.8	931.109 (3)	1396.160	0	3	5	0	C, bisectGN(1030.9)
				f-8 (2)	7644 (A, B)	1492.8	1396.161 (2)	1396.160	0	3	5	0	C, bisectGN(1031.0)
					– (B)	1492.8	979.795 (3)	979.795	1	3	5	0	C, CoreF(1638.9), bisectGN(1031.2), BA-2
				f-9 (2)	7577 (A, B, C)	1492.7	1469.189 (2)	1469.189	1	3	5	0	C, CoreF(1638.8), bisectGN(1031.2), BA-2
					– (A, B, C)	1492.9	1014.806 (3)	1014.806	2	4	4	0	C, CoreF(1640.0), 512(512.3)
				f-1	7558 (A, B, C)	1493.7	1033.813 (3)	1033.813	1	4	5	0	C, bisctGN(1031.1), CoreF(1639.8) or $L^{6'}$ (350.2, 512.2)
					– (A)	1493.8	1550.215 (2)	1550.215	1	4	5	0	C, bisctGN(1031.6), CoreF(1640.0) or 512(512.2)
					– (A)	1492.9	1047.489 (3)	1047.488	1	3	6	0	C, CoreF(1638.8), bisectGN(1031.7)
					– (A, C)	1492.9	1063.151 (3)	1063.151	1	4	4	1	C, CoreF(1638.9)
					– (A)	1492.9	1082.157 (3)	1082.159	0	4	5	1	C, bisectGN(1031.0)
				f-2	**7468 (A, B, C)**	**1492.8**	**1082.499 (3)**	**1082.499**	**2**	**4**	**5**	**0**	**C, CoreF, bisectGN(1103.8) [Figure 5, F1]**
					– (A)	1492.8	1623.243 (2)	1623.244	2	4	5	0	C, CoreF(1638.9), bisectGN(1031.0), 512(513.2)
				f-3	7382 (A)	1492.8	1101.510 (3)	1101.506	1	4	6	0	C, bisectGN(1031.2), CoreF(1639.0) or $L^{6'}$ (350.3, 512.2)
				f-4	7753 (A, B, C)	1492.7	1117.168 (3)	1117.169	1	5	4	1	C, CoreF(1638.8) or $sL^{6'}$ (454.2, 512.3, 657.2, 803.1)
					– (A)	1493.9	1675.247 (2)	1675.250	1	5	4	1	H, CoreF(1638.9)
					– (A)	1493.8	1117.508 (3)	1117.509	3	5	4	0	C, CoreF(1639.4), $L^{6'}$ (512.2, 658.5)
				f-5	7889 (A, C)	1492.8	1130.846 (3)	1130.845	1	4	5	1	C, CoreF(1638.7), bisectGN(1031.0, 1104.3)
					– (A)	1492.9	1136.517 (3)	1136.516	2	5	5	0	C, CoreF(1639.8), 512(512.2)
					– (A)	1494.0	1150.192 (3)	1150.192	2	4	6	0	C, CoreF(1639.1), $L^{6'}$ (350.1, 512.2)
					– (A)	1493.1	1165.516 (3)	1165.515	0	5	4	2	C
				f-6	7815 (A, B, C)	1492.6	1165.856 (3)	1165.855	2	5	4	1	C, CoreF(1638.7), $sL^{6'}$ (453.8, 512.1, 657.1, 803.2)
					– (A)	1493.3	1748.280 (2)	1748.279	2	5	4	1	C, CoreF(1639.9), 512(512.3)
				f-7	7765	1493.9	1184.864 (3)	1184.862	1	5	5	1	C, bisectGN(1032.0), CoreF(1639.3) or 512(512.2)
					– (A, C)	1492.7	1185.202 (3)	1185.202	3	5	5	0	C, CoreF(1639.1), $L^{6'}$ (512.2, 658.4)
					– (A)	1492.7	1204.209 (3)	1204.209	2	5	6	0	C, CoreF(1638.9), $L^{6'}$ (350.2, 512.2)
					– (A, C)	1493.2	1214.201 (3)	1214.201	1	5	4	2	C, CoreF(1639.8)

Table 1: Continued

protein		peptides: sequence[a,b]	glycopeptides: elution position	Figure	peak no.[c]	scan in Figure 4A[d]	observed peptide-related ion[e]	observed m/z in SIM mode[b]	theoretical m/z[b]	N-glycan: deduced monosaccharide composition: dHex	Hex	HexNAc	NA	deduced structure/ (diagnostic ion)
						– (A)	1493.8	1233.548 (3)	1233.548	2	5	5	1	C, CoreF(1639.1), sL$^{x/s}$ (454.0, 512.6, 657.1, 803.0)
						– (A)	1493.8	1287.567 (3)	1287.566	2	6	5	1	C, CoreF(1639.4), 512(512.3)
						– (C)	1492.7	1336.251 (3)	1336.252	3	6	5	1	C, CoreF, 512(512.4)
						- (C)	1492.7	1384.602 (3)	1384.598	2	6	5	2	C, CoreF(1638.8) (sL$^{x/s}$ (454.9, 512.3, 657.1, 803.3))
		LGVTN^{272}ASLVLFRPGSVR (1785.026)	24	5, F2		– (C)	995.3(2)	1096.537 (3)	1096.534	0	3	5	0	C, bisectGN(1279.5)
					g-1	7508 (C)	995.4(2)	1145.223 (3)	1145.220	1	3	5	0	C, CoreF(1068.7), bisectGN(1352.3), BA-2
					g-2	7462 (C)	995.8(2)	1199.243 (3)	1199.238	1	4	5	0	C, CoreF(1069.2) or 512(512.2)
					g-3	7449 (C)	995.9(2)	1247.927 (3)	1247.924	2	4	5	0	C, CoreF(1068.4), bisectGN(1279.4), 512(512.2)
						– (C)	995.8(2)	1282.596 (3)	1282.594	1	5	4	1	C, 512(512.2)
						– (C)	995.4(2)	1331.283 (3)	1331.280	2	5	4	1	C, CoreF(1068.4), 512(512.3)
OBCAM	G	AMDN^{93}VTVR (904.444)	2	6, A2	h-1	2408 (A)	1254.5	1018.407 (3)	1018.405	1	5	3	2	H, CoreF(1254.5), (diSia(583.0))
						– (A, C)	1254.7	1086.098 (3)	1086.099	1	5	4	2	CoreF(1254.7)
						– (A)	1254.5	1628.644 (2)	1628.644	1	5	4	2	C, CoreF(1254.5)
						– (A, B)	1254.7	1115.437 (3)	1115.437	1	5	3	3	H, CoreF(1254.7), diSia(583.0)
						– (A)	1254.5	1672.651 (2)	1672.652	1	5	3	3	H, CoreF(1254.5), diSia(583.3)
						– (A)	1254.6	1169.454 (3)	1169.455	1	6	3	3	H, CoreF(1254.6), diSia(583.0)
					h-2	2473 (A, B, C)	1254.5	1183.131 (3)	1183.130	1	5	4	3	H, CoreF(1254.5) or 512(512.2), diSia(582.6)
					h-3	**2719 (C)**	**1254.5**	**1280.163 (3)**	**1280.162**	**1**	**5**	**4**	**4**	**C, CoreF(1254.5), diSia(582.9) [Figure 6, A1]**
						– (C)	1108.6	1377.198 (3)	1377.194	1	5	4	5	
	A	VAWLN^{43}R (757.424)	11	5, A2		– (B)	961.5	987.930 (2)	987.930	0	5	2	0	Man-5
					a-1 (2)	3523 (A, B, C)	961.5	1068.956 (2)	1068.957	0	6	2	0	Man-6
					a-2 (2)	**3364 (A, B, C)**	**961.5**	**1149.986(2)**	**1149.983**	**0**	**7**	**2**	**0**	**Man-7 [Figure 5, A1]**
					a-3 (2)	3221 (A, B, C)	961.5	1231.010 (2)	1231.010	0	8	2	0	Man-8
					a-4 (2)	3413 (A, B, C)	961.5	1312.039 (2)	1312.036	0	9	2	0	Man-9
		VHLIVQVPPQIMN^{213}ISSD (1889.008)	–	–	–	–	–	–	–	–	–	–	–	glycosylated [f]
		VHLIVQVPPQIMN^{213}ISSDITVNE (2445.294)	–	–	–	–	–	–	–	–	–	–	–	glycosylated [f]
	H	ISTLTFFN^{288}VSE (1256.629)	25	6, B2		– (A)	1460.6	1351.589 (2)	1351.589	1	3	4	0	CoreF(1606.3), bisectGN(1087.8)
						– (B)	1460.5	969.088 (3)	969.088	1	3	5	0	C, CoreF(1606.5), bisectGN(1088.6), BA-2
						– (A, C)	1461.5	1453.128 (2)	1453.128	1	3	5	0	C, CoreF(1606.5), bisectGN(1088.4), BA-2

Table 1: Continued

protein	peptides: sequence[a,b]	elution position	Figure	peak no.[c]	glycopeptides: scan in Figure 4A[d]	observed peptide-related ion[e]	observed m/z in SIM mode[b]	theoretical m/z[b]	N-glycan: deduced monosaccharide composition: dHex	Hex	HexNAc	NA	N-glycan: deduced structure[f] (diagnostic ion)
					− (A, B, C)	1461.7	1071.792 (3)	1071.792	2	4	5	0	C, (CoreF(1606.5), $L^{a/x}$ (350.1, 512.2)) or ($L^{b/y}$ (658.4))
					− (A, C)	1460.5	1607.183 (2)	1607.184	2	4	5	0	C, 512(512.3)
					− (C)	1460.5	1120.138 (3)	1120.137	1	4	5	1	C, CoreF(1606.5)
					− (A, C)	1460.5	1155.148 (3)	1155.148	2	5	4	1	C, CoreF(1606.6) ($sL^{a/x}$ (349.2, 512.2, 804.1)
					− (A, B)	1460.5	1174.494 (3)	1174.495	3	5	5	0	C, CoreF(1606.5), $L^{b/y}$ (350.7, 512.3, 658.2)
					− (A, C)	1461.4	1187.831 (3)	1187.831	1	4	6	1	C, CoreF(1606.6) or $sL^{a/x}$ (350.1, 512.5, 657.1, 803.1)
					− (C)	1460.5	1222.842 (3)	1222.841	2	5	5	1	C, CoreF(1606.5), $sL^{a/x}$ (454.0, 512.2, 803.2)
				i-1	**8712 (A, B, C)**	**1460.5**	**1290.538 (3)**	**1290.534**	**2**	**5**	**6**	**1**	**C, CoreF(1606.6) ($sL^{a/x}$ (454.2, 512.2, 657.1, 803.3) [Figure 6, B1]**
				i-2	8541 (A, C)	1460.5	1393.239 (3)	1393.238	3	6	6	1	C, CoreF(1606.5), 512(512.2)
I	YGN[266]YTCVATNK (1289.571)	7	6, C2		− (A)	1493.6	1254.003 (2)	1254.004	0	5	2	0	Man-5
					− (A)	1493.6	1368.060 (2)	1368.060	1	3	4	0	CoreF(1639.6), bisectGN(1031.5)
					− (B)	1493.6	980.068 (3)	980.069	1	3	5	0	C, CoreF(1639.6), bisectGN(1032.2), BA-2
				j-4 (2)	3156 (A, B, C)	1493.6	1469.602 (2)	1469.599	1	3	5	0	C, CoreF(1639.6), bisectGN(1105.0), BA-2
					− (C)	1493.6	1015.082 (3)	1015.079	2	4	4	0	CoreF(1639.5), $L^{a/x}$ (350.2, 512.1), bisectGN(1105.1)
				j-1	3048 (A)	1494.6	1082.774 (3)	1082.772	2	4	5	0	C, CoreF(1640.5), $L^{a/x}$ (350.4, 512.2), bisectGN(1105.9) **[Figure 6, C1]**
				j-2	3030	1493.6	1117.783 (3)	1117.783	3	5	4	0	H, CoreF(1639.5), $L^{b/y}$ (350.3, 512.1, 658.1)
				j-3	3024	1494.6	1185.478 (3)	1185.476	3	5	5	0	C, CoreF(1639.6), $L^{a/x}$ (349.0, 512.1), bisectGN(1032.7)
	DYGN[266]YTCVATNK (1404.598)	13	−		− (A)	1608.6	1311.517 (2)	1311.518	0	5	2	0	Man-5
					3885 (A)	1609.7	1018.412 (3)	1018.411	1	3	5	0	C, CoreF(1754.5), bisectGN(1089.6), BA-2
					− (A)	1608.6	1527.113 (2)	1527.113	1	3	5	0	C, CoreF(1754.6), bisectGN(1089.1), BA-2
					− (A)	1608.6	1121.115 (3)	1121.115	2	4	5	0	C, CoreF(1754.7), $L^{a/x}$ (350.3, 512.3)
					− (A)	1608.7	1156.125 (3)	1156.125	3	5	4	0	H, CoreF(1754.8), 512(512.2)
	KDYGN[266]YTCVATNK (1532.693)	6	−		− (C)	1736.7	1489.625 (2)	1489.621	1	3	4	0	CoreF(1882.8), bisectGN(1225.1)
					3510 (C)	1737.8	1061.109 (3)	1061.109	1	3	5	0	C, CoreF(1884.9), bisectGN(1226.7), BA-2
					3133	1737.7	1150.141 (3)	1150.137	2	5	4	0	H, CoreF(1883.8), $L^{a/x}$ (350.4, 512.2)

Table 1: Continued

	peptides		glycopeptides						*N*-glycan				
									deduced monosaccharide composition				
protein		sequence[a,b]	elution position	Figure	peak no.[c]	scan in Figure 4A[d]	observed peptide-related ion[e]	observed *m/z* in SIM mode[b]	theoretical *m/z*[b]	dHex	Hex	HexNAc	NA	deduced structure[f] (diagnostic ion)
						– (C)	1736.5	1163.814 (3)	1163.813	2	4	5	0	C, CoreF(1882.7), bisectGN(1153.7), $L^{4/3}$ (350.3, 512.2)
						3054	1737.6	1198.826 (3)	1198.823	3	5	4	0	C, CoreF(1884.7), $L^{4/3}$ (350.1, 512.2)
						3458	1737.1	1212.160 (3)	1212.159	1	4	5	1	C, CoreF(1883.9), bisectGN(1226.3)
						3295	1737.0	1247.170 (3)	1247.169	2	5	4	1	CoreF(1882.8), $sL^{4/3}$ (453.8, 512.2, 657.2, 803.2)
	J	LGNTN[278]ASITLYGPGAVID (1774.910)	–	–		– (A)	1978.7	1093.161 (3)	1093.162	0	3	5	0	C
						– (A)	1979.8	1141.848 (3)	1141.848	1	3	5	0	C, CoreF(1062.9), bisectGN(1273.8), BA-2
neurotrimin	G	AMDN[13]VTVR (904.444)	2	6, A2	h-1	2408 (A)	1254.5	1018.407 (3)	1018.405	1	5	3	2	H, CoreF(1254.5), (diSia(583.0))
						– (A, C)	1254.7	1086.098 (3)	1086.099	1	5	4	2	CoreF(1254.7)
						– (A)	1254.5	1628.644 (2)	1628.644	1	5	4	2	C, CoreF(1254.5)
						– (A, B)	1254.7	1115.437 (3)	1115.437	1	5	3	3	H, CoreF(1254.7), diSia(583.0)
						– (A)	1254.5	1672.651 (2)	1672.652	1	5	3	3	H, CoreF(1254.5), diSia(583.3)
						– (A)	1254.6	1169.454 (3)	1169.455	1	6	3	3	H, CoreF(1254.6), diSia(583.0)
					h-2	2473 (A, B, C)	1254.5	1183.131 (3)	1183.130	1	5	4	3	H, CoreF(1254.5) or 512(512.2), diSia(582.6)
					h-3	**2719 (C)**	**1254.5**	**1280.163 (3)**	**1280.162**	**1**	**5**	**4**	**4**	**C, CoreF(1254.5), diSia(582.9) [Figure 6, A1]**
						– (C)	1108.6	1377.198 (3)	1377.194	1	5	4	5	
	A	VAWLN[36]R (757.424)	11	5, A2	*	– (B)	961.5	987.930 (2)	987.930	0	5	2	0	Man-5
					a-1 (2)	3523 (A, B, C)	961.5	1068.956 (2)	1068.957	0	6	2	0	Man-6
					a-2 (2)	**3364 (A, B, C)**	**961.5**	**1149.986(2)**	**1149.983**	**0**	**7**	**2**	**0**	**Man-7 [Figure 5, A1]**
					a-3 (2)	3221 (A, B, C)	961.5	1231.010 (2)	1231.010	0	8	2	0	Man-8
					a-4 (2)	3413 (A, B, C)	961.5	1312.039 (2)	1312.036	0	9	2	0	Man-9
		GNN[128]ISLTCIATGR (1375.688)	–	–	–	–	–	–	–	–	–	–	–	glycosylated [g]
		GNN[128]ISLTCIATGRPE (1601.783)	–	–	–	–	–	–	–	–	–	–	–	glycosylated [g]
		GNN[128]ISLTCIATGRPEPTVTWR (2285.159)	–	–	–	–	–	–	–	–	–	–	–	glycosylated [g]
	K	LTFFN[252]VSE (955.465)	20	7, A2	k-4 (2)	6885 (A)	1159.4	1086.954 (2)	1086.951	0	5	2	0	Man-5
						– (A)	1159.4	1180.493 (2)	1180.494	1	4	3	0	CoreF(1305.5)
					k-6 (2)	6824 (A, B)	1159.4	1201.011 (2)	1201.007	1	3	4	0	CoreF(1305.4)
						– (A)	1159.5	1261.520 (2)	1261.520	1	5	3	0	H, CoreF(1305.3)
					k-7 (2)	6819 (A, B)	1159.4	1302.551 (2)	1302.546	1	3	5	0	C, CoreF(1305.3), bisectGN(864.6), BA-2
						– (A)	1159.5	1334.551 (2)	1334.549	2	5	3	0	H, CoreF(1305.3), 512(512.3)
						– (A, B)	1159.4	1355.062 (2)	1355.062	2	4	4	0	CoreF(1305.2), 512(512.4)
						– (A, B)	1159.5	1363.059 (2)	1363.060	1	5	4	0	H, bisectGN(864.4), CoreF(1305.4) or 512(511.9)
						– (A)	1160.4	1407.068 (2)	1407.068	1	5	3	1	H, CoreF(1306.4)
						– (A)	1159.8	1415.576 (2)	1415.575	2	6	3	0	H, CoreF(1305.3)

Table 1: Continued

protein	peptides: sequence[a,b]	elution position	Figure	glycopeptides: peak no.[c]	scan in Figure 4A[d]	observed peptide-related ion[e]	observed m/z in SIM mode[b]	theoretical m/z[b]	N-glycan: deduced monosaccharide composition dHex	Hex	HexNAc	NA	deduced structure[f] (diagnostic ion)
					– (B)	1159.4	957.728 (3)	957.728	2	5	4	0	H, CoreF(1305.7), $L^{a/x}$ (350.3, 512.1)
				k-8 (2)	6735 (A, B)	1159.3	1436.093 (2)	1436.089	2	5	4	0	H, CoreF(1305.4), 512(512.3)
					– (A)	1159.7	1444.089 (2)	1444.086	1	6	4	0	H, CoreF(1305.4)
					– (B)	1159.5	971.404 (3)	971.404	2	4	5	0	C, CoreF(1305.4), 512(512.3)
				k-9 (2)	6725 (A, B)	1159.5	1456.605 (2)	1456.602	2	4	5	0	C, (CoreF(1305.4), 512(512.1)) or $L^{b/y}$ (658.2), bisetGN(864.3)
					– (A)	1160.6	1480.098 (2)	1480.097	2	5	3	1	H, CoreF(1305.3), $sL^{a/x}$ (454.3, 512.2, 657.1, 803.2)
				k-1	6590	1159.3	1006.417 (3)	1006.414	3	5	4	0	C, CoreF(1305.2), $L^{b/y}$ (658.3)
				k-2	**6658**	**1159.4**	**1011.747 (3)**	**1011.746**	**2**	**6**	**4**	**0**	**H, CoreF(1305.3), $L^{a/x}$ (350.3, 512.1), bisectGN(865.4) [Figure 7, A1]**
					– (A)	1159.3	1517.117 (2)	1517.115	2	6	4	0	H, CoreF(1305.3), 512(512.1)
					– (A, B)	1160.4	1019.749 (3)	1019.749	1	4	5	1	C, CoreF(1305.4)
					– (A)	1159.5	1054.760 (3)	1054.760	2	5	4	1	H, CoreF(1305.5), 512(512.2)
				k-3	6533	1159.5	1074.108 (3)	1074.107	3	5	5	0	C, CoreF(1305.4), $L^{b/y}$ (658.1)
					– (A)	1159.4	1087.442 (3)	1087.443	1	4	6	1	C, CoreF(1305.4)
					– (A)	1159.5	1122.453 (3)	1122.453	2	5	5	1	C, CoreF(1305.5), 512(512.2)
				k-5	6782 (A, B)	1159.4	1190.151 (3)	1190.146	2	5	6	1	C, CoreF(1305.3), $sL^{a/x}$ (350.2, 512.2, 657.1, 803.2)
	L YGN[168]YTCVASNK (1275.555)	5	7, B2	**l-1**	**2954 (A, B, C)**	**1480.6**	**1078.100 (3)**	**1078.100**	**2**	**4**	**5**	**0**	**C, CoreF(1626.6), bisectGN(1024.9), $L^{a/x}$ (350.3, 512.1) [Figure 7, B1]**
				l-1 (2)	2960 (A)	1479.5	1616.649 (2)	1616.647	2	4	5	0	C, CoreF(1626.6), bisectGN(1024.4), 512(512.2)
				l-2	2918 (A)	1479.6	1113.114 (3)	1113.111	3	5	4	0	H, CoreF(1625.5), $L^{b/y}$ (658.1)
					– (A)	1480.6	1126.446 (3)	1126.446	1	4	5	1	C, CoreF(1626.6)
				l-3	3093	1478.0	1161.457 (3)	1161.457	2	5	4	1	H, CoreF(1626.7), $sL^{a/x}$ (350.4, 512.1, 657.2, 803.1)
				l-4	2905 (A, B)	1479.6	1180.806 (3)	1180.804	3	5	5	0	C, CoreF(1625.6), bisectGN(1024.6), $L^{a/x}$ (350.0, 512.3)
	HDYGN[289]YTCVASNK (1527.641)	8	–		3254 (A, C)	1732.4	1059.426 (3)	1059.425	1	3	5	0	C, CoreF(1878.7), bisectGN(1150.6), BA-2
					3176 (A, C)	1731.6	1162.128 (3)	1162.129	2	4	5	0	C, (CoreF(1878.7), $L^{a/x}$ (350.1, 512.2)) or $L^{b/y}$ (658.4), bisectGN(1223.8)

Table 1: Continued

	peptides		glycopeptides							*N*-glycan				
										deduced monosaccharide composition				
protein		sequence[a,b]	elution position	Figure	peak no.[c]	scan in Figure 4A[d]	observed peptide-related ion[e]	observed *m/z* in SIM mode[b]	theoretical *m/z*[b]	dHex	Hex	HexNAc	NA	deduced structure[f] (diagnostic ion)
						– (C)	1732.7	1197.144 (3)	1197.139	3	5	4	0	H, CoreF(1877.7), $L^{b/y}$ (512.2, 658.2), bisectiGN(1149.1)
						3439	1731.7	1210.475 (3)	1210.475	1	4	5	1	C, CoreF(1877.8), bisectGN(1222.6)
						3383	1732.8	1245.488 (3)	1245.485	2	5	4	1	H, CoreF(1879.7), $sL^{a/x}$ (453.9, 512.2, 657.2, 803.3)
						3080 (C)	1732.7	1264.834 (3)	1264.833	3	5	5	0	C, CoreF(1878.7), bisectGN(1223.4), 512(512.1)
						3553	1731.9	1293.835 (3)	1293.831	1	5	4	2	H, CoreF(1877.6), bisectGN(1150.5)
						3560	1731.9	1294.175 (3)	1294.171	3	5	4	1	C, CoreF(1877.7)
	M	LGHTN[273]ASIMLFGPGAVSE (1799.888)	23	7, C2	m-1	**7299 (C)**	**1002.6(2)**	**1101.491 (3)**	**1101.488**	**0**	**3**	**5**	**0**	**C, bisectGN(1286.7) [Figure 7, C1]**
						– (C)	1003.1(2)	1141.835 (3)	1141.830	0	5	4	0	H, bisectGN(1286.5)
					m-2	7227 (C)	1002.6(2)	1150.176 (3)	1150.174	1	3	5	0	C, CoreF(1075.6), bisectGN(1357.6), BA-2
					m-3	7210	1002.7(2)	1190.520 (3)	1190.516	1	5	4	0	H, CoreF(1075.4) or 512(512.0), bisectGN(1359.1)
					m-4	7186	1002.8(2)	1244.537 (3)	1244.534	1	6	4	0	H, 512(512.2)
Kilon	N	GAWLN[M]R (715.377)	3	8, A2		– (B)	919.5	966.907 (2)	966.907	0	5	2	0	Man-5
					n-1 (2)	**2664 (A, B, C)**	**919.5**	**1047.934 (2)**	**1047.933**	**0**	**6**	**2**	**0**	**Man-6 [Figure 8, A1]**
					n-2 (2)	2706 (A, B, C)	919.5	1128.960 (2)	1128.960	0	7	2	0	Man-7
					n-3 (2)	2679 (A, B, C)	919.4	1209.988 (2)	1209.986	0	8	2	0	Man-8
		CVLEDGASGAWLN[M]R (1738.810)	18	–		5234	972.3	1040.101 (3)	1040.102	0	6	2	0	Man-6
	O	GTN[118]VTLTCLATGXPE (1560.782)	16	8, B2	**o-1**	**4760**	**1765.8**	**1070.475 (3)**	**1070.472**	**1**	**3**	**5**	**0**	**C, CoreF(1910.8), bisectGN(1167.3), BA-2 [Figure 8, B1]**
					o-2	4683	1764.7	1105.485 (3)	1105.483	2	4	4	0	CoreF(1910.9), bisectGN(1167.8), 512(512.2)
					o-3	4710 (C)	1765.7	1173.176 (3)	1173.176	2	4	5	0	C, CoreF(1911.9), bisectGN(1167.3), 512(512.1)
					o-4	4638	1765.8	1275.880 (3)	1275.879	3	5	5	0	C, CoreF(1910.9), 512(512.1)
					o-5	4857 (C)	1765.0	1324.227 (3)	1324.225	2	5	5	1	C, CoreF(1910.8), 512(512.1)
						– (C)	1764.9	1401.911 (3)	1401.910	1	5	4	3	C, CoreF(1911.0)
	P	LFNGQQGIIIQN[138]FSTR (1834.969)	22	8, C2	**p-1**	**7203 (C)**	**1020.3(2)**	**1018.138 (3)**	**1018.138**	**0**	**5**	**2**	**0**	**Man-5 [Figure 8, C1]**
		RLFNGQQGIIIQN[138]FSTR (1991.070)	21	–		6895 (C)	1098.3(2)	1070.171 (3)	1070.172	0	5	2	0	Man-5
		KRLFNGQQGIIIQN[138]FSTR (2119.165)	19	–		6165 (C)	1162.4(2)	1112.871 (3)	1112.870	0	5	2	0	Man-5
	Q	SILTVTN[169]VTQE (1203.635)	17	8, D2	q-8 (2)	5086 (A, C)	1407.5	1211.037 (2)	1211.036	0	5	2	0	Man-5
						– (B)	1407.7	883.729 (3)	883.730	1	3	4	0	CoreF(1553.5), bisectGN(1061.5)

Table 1: Continued

peptides			glycopeptides						N-glycan				
									deduced monosaccharide composition				
protein	sequence[a,b]	elution position	Figure	peak no.[c]	scan in Figure 4A[d]	observed peptide-related ion[e]	observed m/z in SIM mode[b]	theoretical m/z[b]	dHex	Hex	HexNAc	NA	deduced structure[f] (diagnostic ion)
				q-10 (2)	5059 (A, C)	1407.4	1325.094 (2)	1325.092	1	3	4	0	CoreF(1553.5) or 512(512.2), bisectGN(988.6)
					– (B)	1407.6	951.423 (3)	951.423	1	3	5	0	C, CoreF(1553.6), bisectGN(988.6), BA-2
					– (A)	1407.6	1426.632 (2)	1426.631	1	3	5	0	C, CoreF(1553.5), bisectGN(988.2), BA-2
				q-11 (2)	4950 (A, C)	1407.5	1458.635 (2)	1458.634	2	5	3	0	H, CoreF(1553.4), 512(512.2)
					– (B)	1407.3	991.765 (3)	991.765	1	5	4	0	H, CoreF(1553.6)
					– (A)	1407.6	1487.143 (2)	1487.144	1	5	4	0	H, CoreF(1553.4)
				q-1	5126 (A)	1407.5	1021.106 (3)	1021.104	1	5	3	1	H, CoreF(1553.4) or 512(512.2)
					– (A)	1407.6	1531.153 (2)	1531.152	1	5	3	1	H, CoreF(1553.6) or 512(512.0)
				q-2	4885 (C)	1407.4	1026.777 (3)	1026.776	2	6	3	0	H, CoreF(1553.5), $L^{6/3}$ (350.3, 512.2)
				q-2 (2)	4919 (C)	1407.6	1539.663 (2)	1539.660	2	6	3	0	H, CoreF(1554.2), 512(512.1)
				q-3	5010 (A, C)	1407.5	1040.453 (3)	1040.451	2	5	4	0	H, CoreF(1553.6), $L^{6/3}$ (350.2, 512.1)
					– (A)	1407.5	1560.174 (2)	1560.173	2	5	4	0	H, CoreF(1553.4), 512(512.2)
				q-4	**4944 (A, C)**	**1406.6**	**1054.128 (3)**	**1054.127**	**2**	**4**	**5**	**0**	**C, CoreF(1552.6)s, $L^{6/3}$ (350.2, 512.1) [Figure 8, D1]**
					– (A)	1407.6	1580.687 (2)	1580.687	2	4	5	0	C, CoreF(1553.6), 512(512.2)
					– (A)	1407.5	1075.121(3)	1075.122	1	6	3	1	H, CoreF(1554.6)
					– (A)	1407.6	1612.180 (2)	1612.179	1	6	3	1	H, CoreF(1554.5)
				q-5	4827	1407.5	1089.139 (3)	1089.137	3	5	4	0	H, CoreF(1553.6), 512(512.1)
					– (A)	1407.5	1094.469 (3)	1094.469	2	6	4	0	H, CoreF(1554.3), $L^{6/3}$ (350.3, 512.2)
					– (A)	1407.3	1102.473 (3)	1102.473	1	4	5	1	C, CoreF(1552.7)
				q-6	5032	1407.5	1137.486 (3)	1137.483	2	5	4	1	C, CoreF(1553.3), 512(512.2)
				q-7	4869 (A)	1407.6	1156.832 (3)	1156.830	3	5	5	0	C, CoreF(1553.5)
					– (A)	1407.6	1170.166 (3)	1170.166	1	4	6	1	C, CoreF(1553.3) or ($sL^{6/3}$ (512.4, 803.6)
				q-9	5054 (A)	1407.4	1272.870 (3)	1272.869	2	5	6	1	C, CoreF(1553.5) ($sL^{6/3}$ (454.1, 512.2, 657.2, 803.2))
R	HFGN[332]YTCVAANK (1380.624)	10	8, E2		– (B)	793.2(2)	866.690 (3)	866.690	0	5	2	0	Man-5
				r-7 (2)	3214 (C)	1584.7	1299.536 (2)	1299.531	0	5	2	0	Man-5
				r-1	3339 (C)	1584.6	1010.422 (3)	1010.420	1	3	5	0	C, CoreF(1730.6), bisectGN(1077.0), BA-2
				r-2	**3162 (A, C)**	**1584.7**	**1050.764 (3)**	**1050.762**	**1**	**5**	**4**	**0**	**H, CoreF(1730.5), bisectGN(1077.7) [Figure 8, E1]**
				r-3	3139 (A, C)	1585.9	1085.774 (3)	1085.772	2	6	3	0	H, CoreF(1730.8), $L^{6/3}$ (350.2, 512.2)

Table 1: Continued

protein	peptides: sequence[a,b]	glycopeptides: elution position	Figure	peak no.[c]	scan in Figure 4A[d]	observed peptide-related ion[e]	observed *m/z* in SIM mode[b]	theoretical *m/z*[b]	*N*-glycan: deduced monosaccharide composition: dHex	Hex	HexNAc	NA	deduced structure[f] (diagnostic ion)
				r-4	3208 (C)	1585.7	1099.450 (3)	1099.448	2	5	4	0	H, CoreF(1731.7), $L^{a/b}$ (350.1, 512.1)
				r-5	3189	1584.7	1104.784 (3)	1104.780	1	6	4	0	H, CoreF(1730.6) or $L^{a/b}$ (350.4, 512.0)
				r-6	3144 (A)	1585.6	1113.127 (3)	1113.123	2	4	5	0	C, CoreF(1730.8), $L^{a/b}$ (350.1, 512.2)
					– (A)	1585.8	1134.118 (3)	1134.118	1	6	3	1	H, CoreF(1730.6) or 512(512.3)
					– (A)	1584.5	1153.466 (3)	1153.466	2	6	4	0	H, CoreF(1731.6), $L^{a/b}$ (350.1, 512.2)

[a] Theoretical peptide mass indicated in parentheses. [b] Monoisotopic values. [c] Peaks are numbered in decreasing order of their calculated mass. All glycopeptides are triply charged except for doubly charged ions indicated by (2) after the peak number. [d] Glycopeptides were characterized on the basis of alternative LC–MS^n runs with conditions indicated in parentheses (A, a C30 column, scan range of *m/z* 1000–2000; B, a C30 column, scan range of *m/z* 700–2000; C, a C18 column, scan range of *m/z* 1000–2000). [e] $Y_1^{a/b}$ or $Y_{1\alpha/\beta}^{a/b}$, [(peptide + HexNAc + nH)/n]$^{a/b}$; or $Y_{1\alpha}^{a/b}$, [(peptide + HexNAc + dHex + nH)/n]$^{a/b}$. All peptide-related ions are singly charged except for doubly or triply charged ions indicated by (2) or (3). [f] Structures are deduced by MS^n: C, complex-type oligosaccharide; H, hybrid-type oligosaccharide; Man-5-9, high mannose-type oligosaccharide containing 5–9 mannose residues; CoreF, trimannosylcore fucose; bisectGN, bisecting GlcNAc; diSia, disialic acid; $L^{a/b}$, Lewis a/x structure; $sL^{a/b}$, sialylated Lewis a/x structure; $L^{b/y}$, Lewis b/y structure; 512, glycan motif consisting of dHex$_1$Hex$_1$HexNAc$_1$. The structure in parentheses indicates the possible structures to be contained in the glycopeptide. [g] Glycosylation was confirmed by Asn–Asp conversion upon PNGase F digestion.

integrated mass spectrum (peaks f-1–9 and g-1–3 in panel F2 of Figure 5) and their MS/MS spectra suggested that complex-type oligosaccharides including $Le^{a/b}$ or $Le^{b/y}$ -modified and/or bisected oligosaccharides and BA-2 are attached to Asn272 (Table 1F).

(vii) Asn287. The MS/MS spectra of GPI-linked peptides were selected from all MS data on the basis of the GPI-characteristic oxonium ions, such as GlcN-Ino-PO_4^+ (*m/z* 422). The structures of the GPI moieties were characterized from their product ions appearing in the MS/MS spectra, and their peptide portions were identified by comparing their observed masses with the theoretical masses of predicted peptides. Figure 4B shows the TIC obtained by GCC-LC–MS^n for the hydrophilic glycopeptides. On the basis of the presence of GPI-characteristic oxonium ions, the MS data of GPI-linked peptides were located at position 26. The 9.5% of spectra generated at elution position 26 were assigned to those of GPI-linked peptides of LAMP, OBCAM, and neurotrimin.

Figure 5G shows one of the MS/MS spectra acquired at position 26 (precursor ion, $[M + 2H]^{2+}$ at *m/z* 902.5; peak L2 in Figure 4C). On the basis of the GPI-characteristic oxonium ions, such as NH_2Et-PO_4-Man-$GlcN^+$ (*m/z* 447.2), NH_2Et-PO_4-(HexNAc-)Man-$GlcN^+$ (*m/z* 650.3), NH_2Et-PO_4-(HexNAc-)Man-GlcN-Ino-PO_4^+ (*m/z* 910.2), NH_2Et-PO_4-(HexNAc-)(Hex-)Man-GlcN-Ino-PO_4^+ (*m/z* 1072.2), and GlcN-Ino-PO_4^+ (*m/z* 422.2), this peptide was identified as the GPI-linked peptide. The product ion at *m/z* 328.3 was assigned to GlN^{287}-NH-Et^+ on the basis of the fragments that arose by successive cleavages of HexNAc (*m/z* 1600.4), Ino-PO_4 (*m/z* 1340.5), GlcN (*m/z* 1178.3), Man-PO_4-$EtNH_2$ and Hex (*m/z* 732.2), Hex (*m/z* 570.2), and PO_4-Hex (*m/z* 328.3). In addition, the product ions at *m/z* 732.3 and 1072.2 suggested the existence of HexNAc-(NH_2Et-PO_4-)(Hex)-Man3 in the core structure of GPI (inset of Figure 5G). The presence of a positional isomer was inferred from the acquisition of two different MS/MS spectra of GPI-linked peptides (precursor ion $[M + 2H]^{2+}$, *m/z* 903) at different elution times (Table 2). The alternative runs also suggested the presence of a Hex-Man1 and HexNAc-(Hex-)(NH_2Et-PO_4-)Man3 (peak L1, data not shown, Table 2), and a nonsubstituted Man1 and HexNAc-(NH_2Et-PO_4-)Man3 (data not shown, Table 2) in the GPI core structure.

Glycosylation Analysis of OBCAM. OBCAM has six potential N-glycosylation sites at Asn17, -43, -113, -258, -266, and -279, and the predicted linkage site of GPI is Asn295. From the peptide-related ions, peptides eluted at positions 2, 25, and 7 were estimated to be glycopeptides containing Asn17, -258, and -266, respectively (panels A1–C1 of Figure 6). Panels A2–C2 of Figure 6 show the integrated mass spectrum of glycopeptides obtained from positions 2, 25, and 7, respectively. The glycopeptide containing Asn43 is identical to VAWLN^{38}R in LAMP. From the glycosylation at Asn38 in LAMP, Man-5-9 were inferred to be attached to Asn43 (panel A2 of Figure 5 and Table 1A). Although the MS/MS spectrum of the glycopeptide containing Asn113 (VHLIVQVPPQIMN^{113}ISSD) was not acquired, glycosylation at Asn113 was corroborated by detection of VHLIVQVPPQIMD^{113}ISSD after PNGase F treatment (data not shown). The feature of glycosylation at Asn279 was elucidated on the basis of the MS/MS spectra of glycosylated LGNTN^{279}ASITLYGPGAVID which was

Table 2: Summary of GPI Structure in LAMP, OBCAM, and Neurotrimin

protein	peptide (theoretical MW[b])	peak no. in Figure 4C	scan in Figure 4B	GPI-linked peptide: observed peptide-related ion[b] (charge state)	GPI-linked peptide: observed *m/z*[b] (charge state)	GPI-linked peptide: calculated mass	GPI moiety: deduced glycan composition: calculated mass	core	Man1	Man3				theoretical MW[b]
									Hex	Hex	HexNAc	P-EtNH$_2$		
LAMP	CIN[287] (302.3)	L1	3863	328.3 (1)	983.6 (2)	1965.1	1680.9	1	1	1	1	1		1681.3
		L2	3828[c] (Figure5G)	328.3 (1)	902.5 (2)	1803.0	1518.8	1	0	1	1	1		1519.2
			4040[c]	328.3 (1)	903.1 (2)	1804.2	1520.0	1	0	1	1	1		1519.2
			a	328.2 (1)	821.6 (2)	1641.1	1356.9	1	0	0	1	1		1357.0
OBCAM	GVN[295] (288.3)	O1	3701 (Figure6D)	314.3 (1)	976.5 (2)	1951.0	1680.7	1	1	1	1	1		1681.3
		O2	3633[d]	314.3 (1)	895.4 (2)	1788.7	1518.4	1	0	1	1	1		1519.2
			3853[d]	314.3 (1)	895.5 (2)	1788.9	1518.6	1	0	1	1	1		1519.2
		O3	3805	314.3 (1)	814.6 (2)	1627.1	1356.8	1	0	0	1	1		1357.0
neurotrimin	VNN[289] (345.4)	N1	3750	371.2 (1)	1004.8 (2)	2007.7	1680.3	1	1	1	1	1		1681.3
		N2	3741[e]	371.4 (1)	924.0 (2)	1846.1	1518.7	1	0	1	1	1		1519.2
			3896[e]	371.2 (1)	924.1 (2)	1846.1	1518.8	1	0	1	1	1		1519.2
		N3	3873 (Figure7D)	371.3 (1)	842.8 (2)	1683.5	1356.1	1	0	0	1	1		1357.0

[a] The structure of GPI was deduced by another LC–MS[n] run. [b] Average value. [c] Isomers. [d] Isomers. [e] Isomers.

acquired in an alternative run with the C30 column (scan range of *m/z* 1000−2000) (Table 1J).

(i) Asn 17. As shown in panel A1 of Figure 6, the glycopeptide that eluted at position 2 was assigned to AMDN[17]VTVR (and/or AMDN[12]VTVR in neurotrimin) glycosylated with $dHex_1Hex_5HexNAc_4NeuAc_4$ based on the $Y_{1\alpha}$ ion and the monoisotopic mass of the molecular ion. The attachment of three NeuAc residues in one branch of a biantennary complex type was suggested by the existence of characteristic B ions (*m/z* 495.2, 744.9, and 1239.2) (panel A1 of Figure 6). The molecular ions appearing in the integrated mass spectrum and their MS/MS spectra suggested that most of the glycans at Asn17 were disialic acid-conjugated oligosaccharides (peaks h-1−3 in panel A2 of Figure 6 and Table 1G).

(ii) Asn258. Panel B1 of Figure 6 shows the representative MS/MS spectrum of glycosylated ISTLTFFN[258]VSE that eluted at position 25. The monosaccharide composition ($dHex_2Hex_5HexNAc_6NeuAc_1$) implied two possible structures: a sLe$^{a/x}$ -modified core-fucosylated complex type and a Le$^{a/x}$ or antigen H-modified core-fucosylated and sialylated complex type (inset of panel B1 of Figure 6). The molecular ions (peaks i-1−2) in the integrated mass spectrum (panel B2 of Figure 6) and the detection of nonglycosylated ISTLTFFN[258]VSE revealed that Asn258 is partly glycosylated with the sLe$^{a/x}$ or Le$^{b/y}$-modified core-fucosylated complex type, and BA-2 (Table 1H).

(iii) Asn266. Panel C1 of Figure 6 shows the product ion spectra of the glycopeptide at position 7, the peptide portion of which was assigned to YGN[266]YTCVATNK on the basis of the $Y_{1\alpha/\beta}$ ion in the MS/MS/MS spectrum. The glycan was characterized as the bisected and core-fucosylated complex-type oligosaccharide containing Le$^{a/x}$ structure from the monosaccharide composition ($dHex_2Hex_4HexNAc_5$), and the Le$^{a/x}$-, bisecting-, and core-fucose-related ions. The MS/MS spectra acquired with other glycoforms (peaks j-1−4 in panel C2 of Figure 6) together with the MS/MS spectra of the glycopeptides DYGN[266]YTCVATNK (position 13) and KDYGN[266]YTCVATNK (position 6) suggested that the Le$^{a/x}$-modified and/or bisected complex type and Man-5 were predominantly attached to Asn266 (Table 1I).

(iv) Asn295. On the basis of the GPI-characteristic oxonium ions and the peptide-related ion (*m/z* 314.3), the MS/MS spectrum of GPI-linked GVN[295] was picked out from position 26 (Figure 6D; precursor ion, *m/z* 976.5; peak O1 in Figure 4C). The fragments arising from the GPI moiety suggested the linkage of Hex to Man1, and HexNAc, Hex, and $NH_2Et\text{-}PO_4$ to Man3 in the core structure (Figure 6D, inset). Furthermore, the MS/MS spectrum of other GPI-linked GVN[295] (precursor ion, *m/z* 895; peak O2), which was picked out from position 26 based on the peptide-related ion, suggested that this GPI moiety contained HexNAc-(Hex)-($NH_2Et\text{-}PO_4$-)Man3. Another MS/MS spectrum (precursor ion, *m/z* 814; peak O3) suggested the linkage of GPI moieties containing HexNAc-($NH_2Et\text{-}PO_4$-)Man3 (Table 2). The existence of two isomers was suggested in peak O2 by the acquisition of two MS/MS spectra of GPI-GVN[295] (*m/z* 895) at different elution times.

Glycosylation Analysis of Neurotrimin. Neurotrimin contains seven potential N-glycosylation sites at Asn12, -38, -120, -184, -252, -260, and -273, and the predicted linkage site of GPI is Asn289. As the amino acid sequence in the